

Kinematics of Ionised Gas in the Barred Seyfert Galaxy NGC 4151

M. W. Asif¹, C. G. Mundell² & A. Pedlar¹

¹ Jodrell Bank Observatory, School of Physics and Astronomy, University of Manchester, Macclesfield, Cheshire SK11 9DL

² Astrophysics Research Institute, Liverpool John Moores University, Twelve Quays House, Birkenhead L41 1LD

29 January 2019

ABSTRACT

We have determined the structure and kinematics of ionised gas in the weak oval bar of the archetypal Seyfert 1 galaxy, NGC 4151, using the TAURUS Fabry-Perot interferometer to simultaneously map the distribution and kinematics of H β emission. We also present broad-band ultraviolet imaging of the host galaxy, obtained with XMM-Newton, that shows the detailed distribution of star formation in the bar and in the optically-faint outer spiral arms. We compare the distribution and kinematics of ionised gas with that previously determined in neutral hydrogen by Mundell & Shone; we suggest that the distribution of bright, patchy UV emission close to the H I shocks is consistent with ionisation by star clusters that have formed in compressed pre-shock gas. These clusters then travel ballistically through the gaseous shock to ionise gas downstream along the leading edge of the bar. In addition, we detect, for the first time, ionised gas within the shock itself which is streaming to smaller radii in the same manner as the neutral gas.

Key words: galaxies: active - galaxies: individual: NGC 4151 - galaxies: ISM - galaxies: kinematics and dynamics - galaxies: Seyfert - galaxies: spiral

1 INTRODUCTION

Present in at least 58% of nearby galaxies, bars are thought to be ubiquitous in galaxies in the local Universe (e.g. Mulchaey & Regan 1999; Menendez-Delmestre et al. 2004). Bars may play a key role in triggering star formation (e.g. Martinet & Friedli 1997; Reynaud & Downes 1999; Sheth et al. 2002) and at higher redshift, may form bulges and drive galaxy evolution (e.g. Norman, Sellwood & Hasan 1996). Their role in the triggering and fuelling of nuclear activity in Active Galactic Nuclei (AGN) is still unclear but bars may offer a useful mechanism for transporting gas towards the centres of galaxies (Roberts, Huntley & Van Albada 1979; Schwarz 1985; Shlosman, Frank & Begelman 1989; Sakamoto et al. 1997), for example when gas streamlines associated with different orbit families converge and form shocks that dissipate angular momentum, thereby allowing gas to move to smaller radii (Prendergast 1983; Athanassoula 1992a,b). Dust lanes were long-considered circumstantial evidence for the presence of such gaseous shocks but direct kinematic evidence was difficult to obtain due to the small amounts of ionised gas associated with them (e.g. Lindblad & Joersäter 1988; Lindblad, Lindblad & Athanassoula 1996). Subse-

quent high angular resolution radio studies of neutral hydrogen in the nearby barred Seyfert, NGC 4151 (Mundell & Shone 1999) provided strong kinematic evidence for streaming shocks in a weak barred potential, as predicted by numerical simulations (Athanassoula 1992a,b).

NGC 4151 is a nearby grand-design barred spiral galaxy, classified as (R')SAB(rs)ab (de Vaucouleurs et al. 1991), with a Seyfert type 1.5 active nucleus (Osterbrock & Koski 1976). Optically, the 3' \times 2' oval bar and active nucleus are the most prominent features, with two faint outer spiral arms that show little evidence of star formation and are visible only in deep optical images (Arp 1977). A string of HII regions lie along the NW and SE leading edges of the bar (Schulz 1985). Low-excitation ionised gas associated with these HII regions was detected in H α +N[II] narrow-band images by Pérez-Fournon & Wilson (1990), along with high-excitation gas in the Narrow Line and Extended Narrow Line Regions (NLR/ENLR) that is photo-ionised by hard ultraviolet radiation from the AGN.

Despite the lack of star formation beyond the bar, the faint outer spiral arms are gas rich and are prominent in neutral hydrogen images, beginning at each end of the oval bar and winding out to a radius of 6 arcmins (\sim 23 kpc)

(Davies 1973; Bosma, Ekers & Lequeux 1977; Pedlar et al. 1992; Mundell et al. 1999). The oval bar is also unusually gas rich (Pedlar et al. 1992; Mundell et al. 1999) and was studied in detail by Mundell & Shone (1999) who demonstrated that the gas dynamics of the oval are consistent with those of a kinematically weak bar. Mundell & Shone (1999) identified sharp velocity changes across bright regions close to the leading edges of the bar, concluding that these regions represent offset shocks, as predicted by simulations of gas flows in barred potentials (Athanassoula 1992a,b), which have formed due to the convergence of gas orbital streamlines associated with the two families of stellar orbits, x_1 and x_2 , that must be present in the bar.

In this paper we present a study of the distribution and kinematics of ionised gas in the arcminute-scale bar of NGC 4151 using observations of the UV continuum emission at $\lambda=2905$ Å obtained with the UVOT on board XMM-Newton and H β emission obtained with the TAURUS Fabry-Perot interferometer on the Isaac Newton Telescope (INT). The advantage of TAURUS over long-slit spectroscopy (e.g. Unger et al. 1987) or narrow band imaging (Pérez et al. 1989) is that it simultaneously provides both complete spatial coverage with a large field of view and two-dimensional kinematic information (at intermediate velocity resolution). Fabry-Perot interferometers have been used successfully to study the distribution and kinematics of ionised gas in a number of active galaxies (e.g., NGC5128 - Bland, Taylor & Atherton 1987; NGC1275 - Unger et al. 1990; NGC1068 - Cecil, Bland & Tully 1990; Unger et al. 1992) and here we present the first Fabry-Perot observations of H β emission from NGC 4151.

The paper is structured as follows: the observations and data reduction are presented in Section 2, the properties of the ultraviolet continuum and ionised gas are described in Section 3 and compared with previous optical observations of this galaxy. In Section 4, we place our results in the context of barred-galaxy gas-dynamic studies by comparing the distribution and kinematics of the ionised gas with those previously derived by Mundell & Shone (1999) for neutral hydrogen in NGC 4151, concentrating particularly on the behaviour of the ionised gas in the vicinity of the HI shocks that Mundell & Shone (1999) identified along the leading edges of the oval bar.

For consistency with previous studies, we use a value of 13.3 Mpc ($H_0=75$ km s $^{-1}$ Mpc $^{-1}$) for the distance to NGC 4151. However, we note that the true distance is likely to be greater given its membership of the Virgo Cluster (see Mundell et al. 1999 for full discussion) and distance-dependent quantities derived in this paper are therefore lower limits.

2 OBSERVATIONS & DATA REDUCTION

2.1 Ultraviolet Continuum Imaging

We obtained archival ultraviolet images taken on 2000 December 22 and 23 (P.I. Griffiths) with the optical monitor on XMM-Newton in the UVW1 ($\lambda_c\sim2905$ Å, $\Delta\lambda\sim620$ Å) filter (see Mason et al. 2001). The total exposure time was 10.8 ks, the pixel size is 0''.95 and the data were processed using SAS version 5.4. Measured counts in the final

Table 1. TAURUS H β observational parameters.

Date of Observation	1989 February 25
Integration time(s)	3200
Etolon Gap (μ m)	76.996
Wavelength of order-sorting filter (Å)	4883
Bandpass of order-sorting filter (Å)	15
Order of interference	315
Free Spectral Range (Å)	15.45
Spectral scale (Åpixel $^{-1}$)	0.175
FWHM spectral resolution (Å)	0.65
Spatial scale (arcsec pixel $^{-1}$)	0.56
FWHM spatial resolution (arcsec)	1.82
Field of view (arcsec 2)	196 × 196

median-combined image were converted to flux units using a value averaged over different spectral types as listed in Section 7.1.2.8 (Method 2 by Breeveld) in the SAS Watchout documentation*.

2.2 TAURUS H β observations

Observations of the H β 4861Å line emission from NGC 4151 were obtained at the f/15 Cassegrain focus of the 2.5-m Isaac Newton Telescope (INT) using the original version of the TAURUS scanning Fabry-Perot interferometer instrument (Taylor & Atherton 1980; Atherton et al. 1982). The observations used the blue-sensitive IPCS detector (Boksenberg 1982) which was not well suited to H α (6563Å) observations. The 75μm etalon used had a free spectral range (FSR) of 15.45Å (953.4 kms $^{-1}$) and was rapidly scanned in steps of 0.175Å (10.800 kms $^{-1}$) with the data being summed into a three-dimensional data cube with 350 × 350 pixels (of 0.56 arcsecs 2 each) in the spatial dimension and 100 pixels in the spectral dimension. The limited FSR of TAURUS also meant that it would be problematic to separate H α from [NII]6583Å lines and thus H α was not observed.

The TAURUS data were reduced using TAUCAL (Lewis & Unger 1991) running within the FIGARO and NDPROGS environments of the STARLINK package. The data were first phase-calibrated (Atherton et al. 1982) relative to exposures of a neon arc source taken before the galaxy exposures and then smoothed in order to improve the signal-to-noise ratio. Gaussian profiles were then fitted using TAU_FITS, a routine within TAUCAL, which gave an estimate of the intensity, central wavelength, width and continuum level for each pixel with line emission. Finally, maps of the intensity distribution, velocity field and velocity dispersion were derived after fitting each of the spectra. Unfortunately, the complex wavelength calibration used for TAURUS data cubes does not enable accurate flux calibration or line ratios to be achieved. The observational parameters and final spatial and spectral resolutions for the H β data are summarised in Table 1.

3 RESULTS & ANALYSIS

The oval bar and AGN are bright at ultraviolet wavelengths; fainter UV emission is also detected coincident

* (see

http://xmm.vilspa.esa.es/external/xmm_sw_cal/sas.shtml

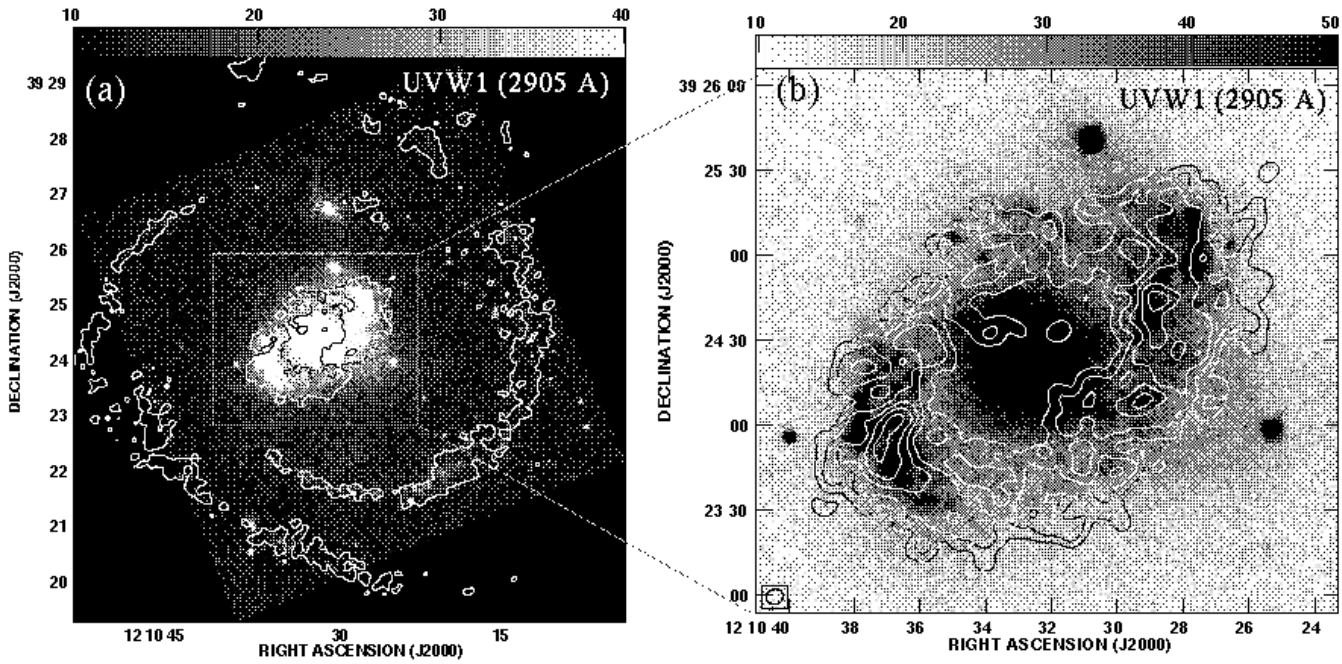


Figure 1. XMM-Newton ultraviolet image of NGC 4151 in the UVW1 filter with HI contours from Mundell et al. (1999) overlaid: (a) whole galaxy (b) oval bar region. The flux density scale is shown at the top of each image in units of $10^{-16} \text{ erg s}^{-1} \text{ cm}^{-2} \text{ \AA}^{-1}$; HI contour levels correspond to column densities (a) $N_H = 0.4 \times 10^{21} \text{ cm}^{-2}$ and (b) $N_H = (0.3, 0.8, 1.8, 2.8, 3.6) \times 10^{21} \text{ cm}^{-2}$ and the beam-size is $6'' \times 5''$.

with the outer spiral arms, particularly towards the bluer south/south-west arm. Within the oval bar, spatially-resolved H β emission is detected from three main regions: faint emission from HII regions that lie along the NW and SE leading edges of the bar and stronger emission associated with NLR and ENLR, elongated along P.A. $\sim 48^\circ$, consistent with structures identified in earlier H α +N[II] narrow-band images (e.g. Pérez-Fournon & Wilson 1990).

3.1 Ultraviolet Continuum Emission

Figure 1 shows XMM-Newton ultraviolet continuum images in the UVW1 (2905 Å) filter of NGC 4151, with contours of HI emission overlaid to illustrate the structure of the galaxy. As can be seen in Figure 1(a), the oval bar and AGN are prominent but faint emission from the outer spiral arms is also detected. Ultraviolet continuum emission from the spiral arm that begins at the SE end of the bar can be followed to more than half way along its length, while faint patches associated with arm that begins at the NW end of the bar can be seen particularly towards its southern-most tip; the ultraviolet continuum is well traced by the HI structures, suggesting that star formation is occurring at a low level in the regions of highest HI column density and that the neutral gas is porous.

In the bar, the bright regions associated with the HII regions along the NW and SE leading edges are prominent (Figure 1(b)) and broadly coincide with the regions of highest HI column density. Fainter, diffuse ultraviolet emission is present across the entire bar and despite its patchy nature,

the UV emission clearly delineates two curved arms winding clockwise from the leading edges of the bar in towards the nucleus, in a remarkably similar way to that observed in HI (Mundell & Shone 1999; Mundell et al. 1999). The total luminosities, L_{UV} (uncorrected for extinction), measured in two elliptical apertures (semi-major axis $27''.6$, ellipticity 0.73) centred on the NW and SE HII regions are $L_{UV} \sim 1.5$ and $1.2 \times 10^{38} \text{ erg s}^{-1} \text{ \AA}^{-1}$ respectively. Archival ultraviolet images of NGC 4151 taken with the Ultraviolet Imaging Telescope (UIT) are not sensitive to the faint UV emission in the spiral arms but do confirm the structure and blue colour of the bar HII regions as seen in our XMM-Newton image (e.g. Fanelli et al. 1997; Kuchinski et al. 2000).

3.2 H β Emission

Figure 2 shows channel maps from the TAURUS H β cube covering the $3' \times 2'$ oval bar; H β emission is detected from the AGN in all velocity channels, consistent with the large line-width of the nuclear emission (Robinson et al. 1994). H β emission associated with the NLR and ENLR is detected along P.A. $\sim 48^\circ$ over the velocity range $854\text{--}1123 \text{ km s}^{-1}$ out to a radius of $\sim 25''$ from the nucleus. Finally, faint clumpy H β emission can be seen NW and SE of the nucleus over the velocity range $945\text{--}1082 \text{ km s}^{-1}$, coincident with the bar HII regions discussed in the previous section. No correction for stellar absorption in the H β emission line profiles has been applied since the narrow free spectral range (15Å) of TAURUS means that the data are insensitive to any broad absorption line components similar to that detected in

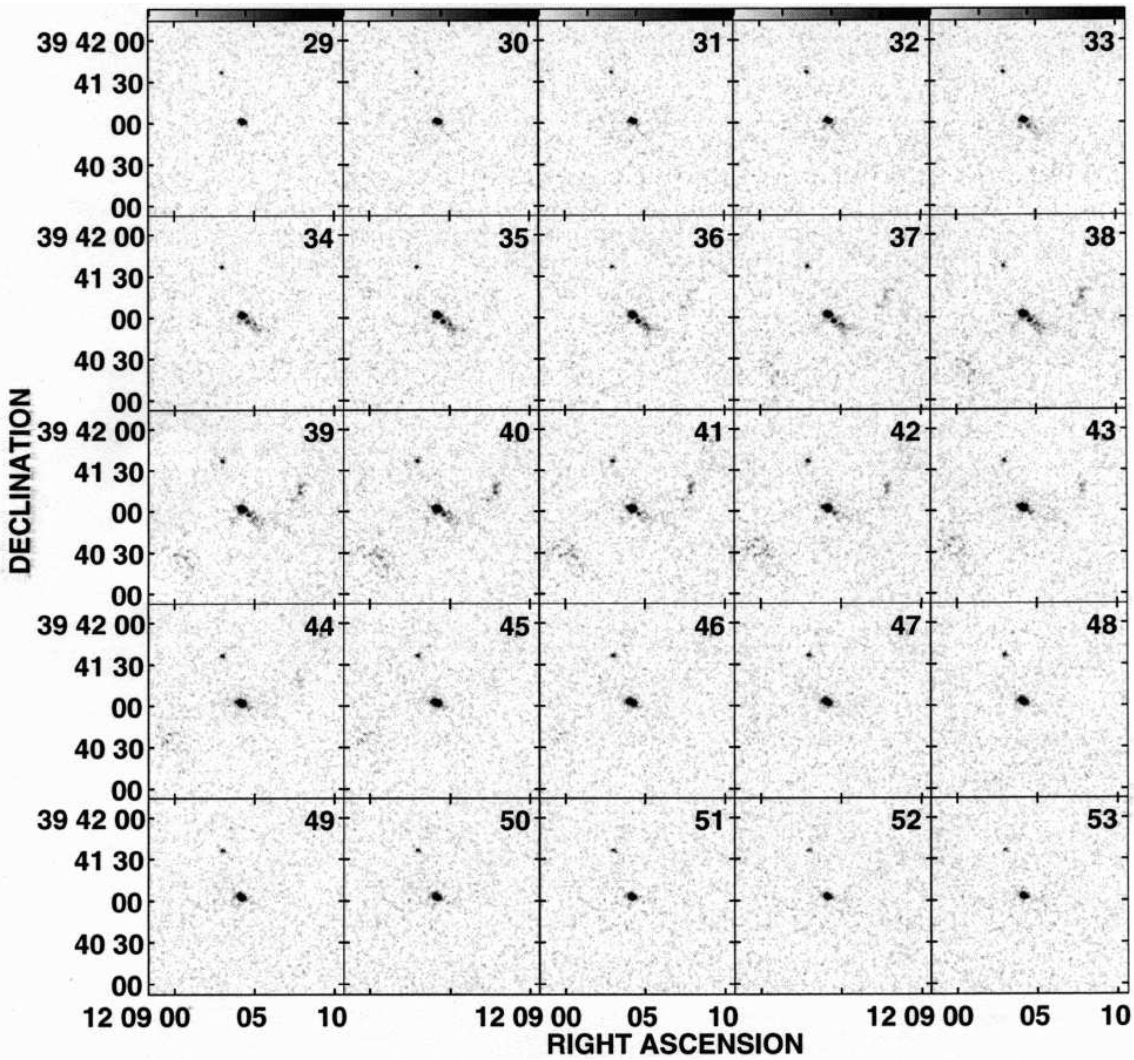


Figure 2. H β velocity channel maps of the HII regions in NGC 4151. The range of values are 946 kms $^{-1}$ to 1065 kms $^{-1}$ with channel 41 corresponding to 998 kms $^{-1}$. North is up and East to the left.

NGC 1068 (FWZI \sim 80Å) by Bland-Hawthorn, Sokolowski & Cecil (1991). To verify this, we inspected the NGC 4151 H β line profiles in long-slit spectra published by Robinson et al. (1994) in which there is no comparable absorption component. We therefore conclude that any H β stellar absorption will not have a significant effect on our H β image and derived kinematics.

3.2.1 The HII Regions

Figure 3 shows representative spectra of the H β emission in the NW and SE regions of the bar. The ultraviolet continuum and HI is also shown for comparison. Although the UV continuum structure is broadly consistent with two arc-like arms along the leading-edges of the bar (Figure 1(b)), the detailed structure is more complicated. The brightest

structures in the NW region consist of two dislocated arcs, labelled NE1 and NE2 in Figure 3, while the bright structure in the SE region resembles an Ω -like ridge (see also Schulz 1985), each side of which we label SE1 and SE2 (Figure 3).

As can be seen in the H β moment map in Figure 4(b), which was derived by fitting Gaussian profiles to each spectrum in the cube, ionised gas is detected in each of these four bright continuum segments, NW1, NW2, SE1, SE2. The H β kinematics are also consistent with those derived from earlier optical long-slit spectroscopy; Figure 5 shows a comparison between velocities derived by Schulz (1985) from long-slit spectra of the brightest knots in the NW and SE HII regions and those derived from the TAURUS H β cube. Radial velocities are plotted as a function of azimuthal angle, with the AGN at the origin.

Figure 6 shows HI iso-velocity contours from Mundell et

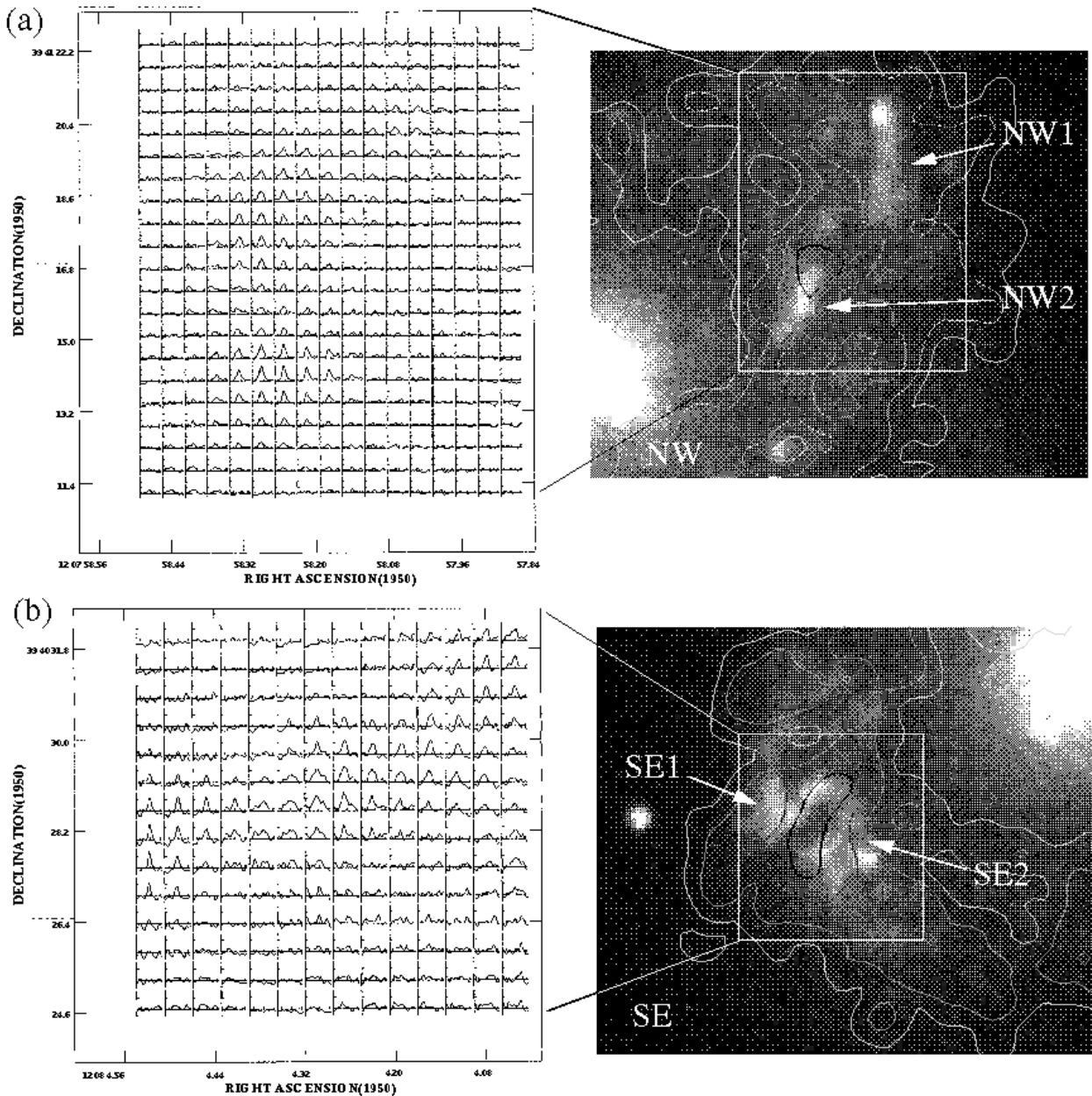


Figure 3. Left: H β spectra of the HII regions along the (a) north-west and (b) south-east edges of the bar. Each spectrum covers a velocity range of 900 – 1100 km s $^{-1}$. Right: the UV image of each region with HI intensity contours overlaid to illustrate the structure of the regions in which H β emission is detected. Individual bright segments in each region are labelled NW1, NW2, SE1 and SE2 (see text for discussion).

al. (1999) overlaid on the H β velocity map smoothed to the same angular resolution ($6'' \times 5''$); it is clear that the ionised gas velocities in the bar HII regions closely resemble the cold gas kinematics which are dominated by rotation within the galactic potential (see also Figure 5 of Mundell et al. 1999). The larger concentration of HI in the bar compared to ionised gas helps to provide a context in which to understand the ionised gas features. Firstly, the arc of neutral gas along the NW edge of the bar appears to join smoothly to the

ionised gas at the SE tip of the ENLR, with ionised and neutral gas velocities and line-widths matching closely (Asif et al. 1997); this continuity suggests a spatial and dynamical link between the neutral and ionised gas and transportation of gas towards the AGN (Mundell & Shone 1999). A similar correspondence between the NW HI and ultraviolet arc can be seen in Figure 1(b).

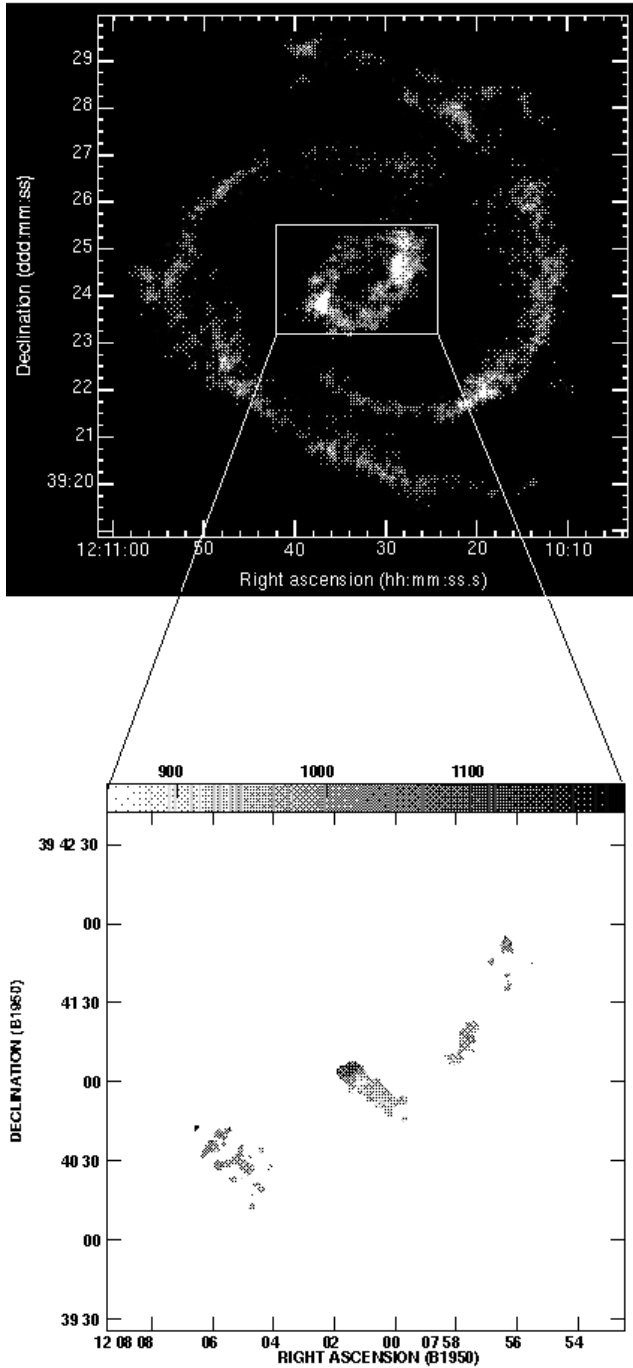


Figure 4. (a) The HI intensity distribution of NGC 4151 from zeroth moment analysis (Mundell et al. 1999). (b) The velocity distribution of H β emission line gas in the nucleus of NGC 4151 derived from TAURUS observations. The range of values are 854–1197 km s $^{-1}$.

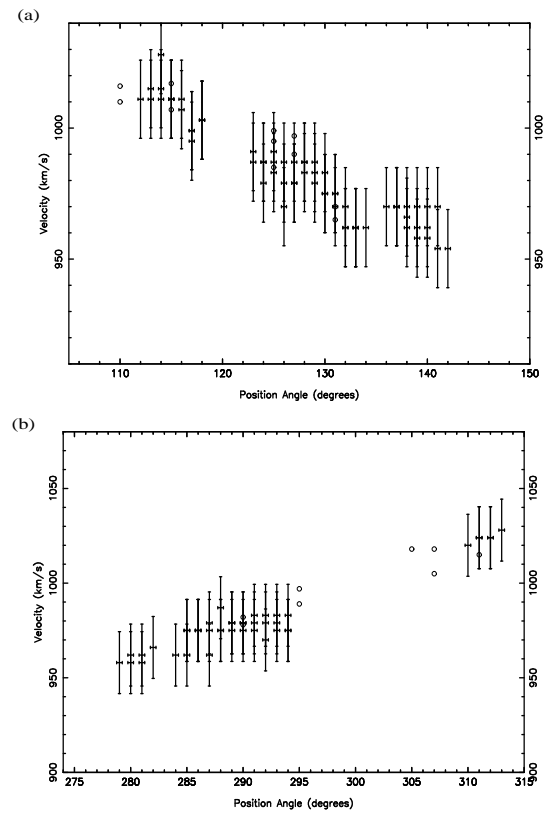


Figure 5. Optical velocities of the (a) SE and (b) NW HII regions in NGC 4151. The velocities were measured through azimuthal angles from the nucleus. TAURUS H β velocities are denoted by crosses and agree well with velocity measurements from Schulz (1985) (open circles).

3.2.2 The Extended Narrow Line Region

The ENLR in NGC 4151 has already been well-studied using both narrow-band imaging (e.g. Pérez-Fournon & Wilson 1990) and long-slit spectroscopy (e.g. Unger et al. 1987; Asif et al. 1997). Our 2-D TAURUS observations are consistent with these previous studies. The velocity profile along the axis of the ENLR was extracted by interpolating the velocity field across the nucleus; a systemic velocity of 1000 ± 2 km s $^{-1}$ was derived, consistent with the value of 998 km s $^{-1}$ derived by others (Pedlar et al. 1992; Mundell et al. 1999; Robinson et al. 1994; Asif et al. 1997; Winge et al. 1999).

The H β emission lines in the ENLR (i.e. at distances greater than $5''$ from the nucleus) are narrow (FWHM < 25 km s $^{-1}$) and consistent with galactic rotation (see also Pedlar et al. 1992; Robinson et al. 1994; Vila-Vilaró et al. 1995; Asif et al. 1997; Winge et al. 1999). Indeed, as shown in Figure 4(b) there is a clear distinction between the velocity structure of the NLR, which is dominated by outflow (e.g. Hutchings et al. 1999; Crenshaw et al. 2000) and the ENLR. However, our TAURUS data show some evidence for additional velocity structure within the SW ENLR, with measured deviations from circular velocity of up to 20 km s $^{-1}$, which could correspond to much higher intrinsic velocities when corrected for galactic inclination. Evidence for a relatively wide angle cone (opening angle of ~ 120 degrees) partially intercepting the galactic disk (to produce

$1''$ at least. This is adequate for comparison with the HI emission which has an angular resolution of $\sim 6''$.

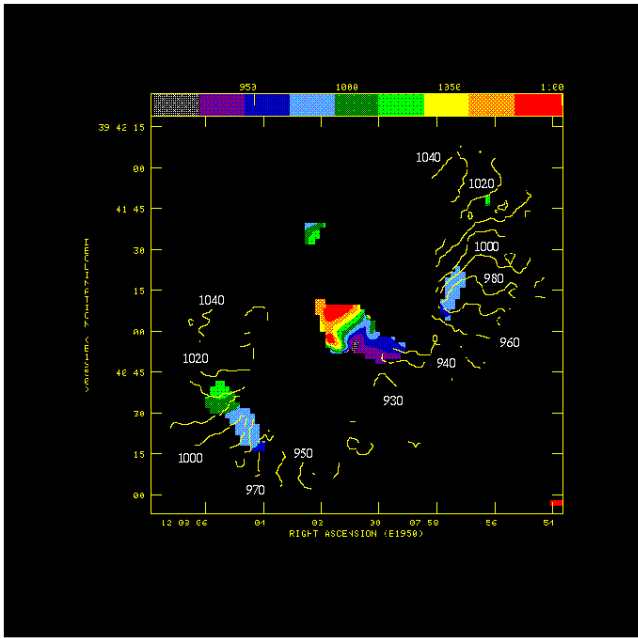


Figure 6. Comparison of $H\beta$ (colour) and HI velocities (contours) of the bar region in NGC 4151. The velocities are in km s^{-1} .

the ENLR) has been discussed extensively by Pedlar et al. (1992), Robinson et al. (1994) and Vila-Vilaró et al. (1995).

4 DISCUSSION

The location of ionised gas ($H\alpha$), molecular gas (CO) and dust in barred galaxies is often observed to be offset along the leading edge of the host stellar bar (e.g. Martin & Friedli 1997; Ondrechen 1985; Handa et al. 1990; Regan & Vogel 1995; Reynaud & Downes 1998). Sheth et al. (2002) find a further offset between the distribution of molecular gas and HII regions as traced by $H\alpha$ emission, with the $H\alpha$ emission generally offset towards the leading edge of the CO emission, and the largest offsets found in the strongest bars. These offsets are interpreted broadly as evidence for stellar clusters forming in compressed pre-shock gas or molecular cloud complexes upstream from the shock; these stellar clusters then travel through the shock ballistically on elliptical orbits and ionise the post-shock gas. This is in contrast to the dissipative neutral or molecular gas in the bar that is focussed and redirected inwards when it meets the shock. In NGC 4151, although no published detection of molecular gas in the bar exists, neutral hydrogen is sharply focussed and streams inwards along the leading-edge shocks (Mundell & Shone 1999). Here we examine the distribution and kinematics of the ionised gas with respect to that of the neutral gas and discuss whether obscuration, kinematics or a combination of both might explain the observed features. In these observations, the optical astrometry was tied to the position of the continuum nucleus of NGC 4151 and was accurate to

4.1 Origin of Ionised Gas in the Bar Shocks

Overall, the UV light distribution in the bar of NGC 4151 is patchy; the whole bar is filled with diffuse UV light, with the bright HII regions along the leading edges of the bar standing out clearly. Spurs and knots of UV emission are also evident close to the minor axis of the bar, particularly $\sim 45''$ north of the galaxy nucleus. As shown in Figures 1(b) and 3, the HII regions in the bar are concentrated around the HI shocks; in the SE, the small arc of highest HI column density is coincident with the dark region in the Ω -shaped ridge, so that the bright UV/ $H\beta$ -emitting regions SE1 and SE2 straddle the HI ridge. In the NW, the two bright UV ridges, NW1 and NW2 are similarly separated by an apparent dust lane that lies along the HI shock; specifically, the NW1 UV ridge is located azimuthally downstream of the HI shock ridge. However, the NW2 ridge appears to line up closely with that of the HI, although the actual emission peaks do not coincide identically.

The patchy nature of the UV light may in part be explained by extinction. Assuming the HI forms a screen in front of the UV emission, the maximum amount of obscuration due to the HI, which has a peak column density in the shocks $N_H = 3.6 \times 10^{21} \text{ cm}^{-2}$, corresponds to 4.9 magnitudes of extinction at $\lambda=2905\text{\AA}$ (assuming a Galactic extinction law; Staveley-Smith & Davies 1987). However, mixing of the gas and stars is more likely making this value an upper limit. Nevertheless, obscuration in the HI shocks, which are also likely to be dust-rich, may partially explain the patchy UV emission and the appearance that the ionised-gas/UV-bright regions are straddling/bracketing the HI shocks, particularly in the SE. The likely effect of dust on the $H\beta$ profiles is difficult to tell due to the lack of any $H\alpha$ data. The profiles shown by Robinson et al. (1994) do not show significant differences between the two lines and we do not expect the effect to change the kinematics dramatically. However, these profiles are not from the shocked regions and also have relatively poor velocity resolution (90 km s^{-1} to 420 km s^{-1}). A better test for this effect would be to use high velocity resolution (6 km s^{-1}) echelle spectroscopy of both $H\alpha$ and $H\beta$ with high signal-to-noise.

Alternatively, dynamical effects may explain the distribution of ionised gas. Mundell & Shone (1999) showed that the neutral hydrogen is distributed throughout the oval bar, with strong streaming motions concentrated along the highest column density HI ridges, evident in the residual velocity field derived by removing the circular rotation component, and confirming their identification as leading-edge shocks. N-body/SPH simulations by Sheth et al. (2002) showed that compression of gas clouds travelling into the shock region can trigger star formation upstream of the shock; these stellar clusters then travel ballistically through the shock region, unlike the gas which is channelled inwards along the shock towards the nucleus, to ionise ambient gas beyond the shock. Taking a lifetime of an HII region to be 3 Myr (Spitzer 1978), Sheth et al. (2002) assume a lifetime of 10 Myr for the $H\alpha$ emission which represents a spread in HII region ages given that individual HII are not spatially resolved.

For NGC 4151, we use the bar pattern speed

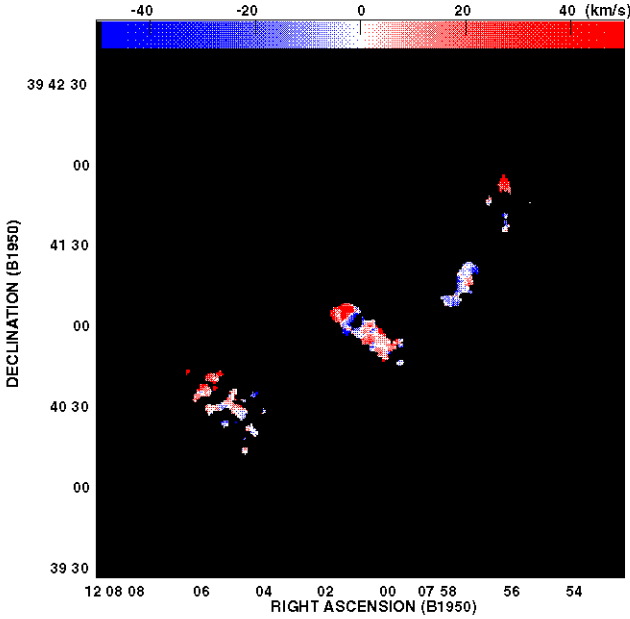


Figure 7. $\text{H}\beta$ residual velocity field; colour scale units are km s^{-1} .

$24.5 \text{ km s}^{-1} \text{ kpc}^{-1}$ and galaxy rotation speed derived by Mundell et al. (1999) to derive the speed at which newly-formed stars will enter the bar shocks, at $\sim 3.9 \text{ kpc}$ from the galaxy centre. For a lifetime of 10 Myr, consistent with the UV luminosity, the maximum distance travelled is 1.2 kpc or $18''$. This distance is consistent with the total extent of the ionised gas across both shock regions. To further test this dynamical scenario we compared the 2-D ionised gas velocities measured in our TAURUS cube with those measured by Mundell & Shone (1999) for the HI; as shown in Figure 6, the HI and $\text{H}\beta$ velocities are consistent and are therefore dominated by the rotation of the galaxy. In order to examine departures from circular rotation we derived an ionised gas residual velocity field using the same method that Mundell & Shone (1999) used to derive the HI residual velocity field (their Figure 2). We used the HI rotation curve (Mundell et al. 1999) to derive a 2-D model velocity field which was then subtracted from the ionised gas velocity field to leave the residual velocity field shown in Figure 7. We have applied the same colour table as that used by Mundell & Shone (1999) to allow a direct comparison of ionised and neutral gas velocity residuals. Although spatial coverage of the ionised gas is limited compared with that of the neutral gas, it is clear that the two residual fields are consistent; comparison of the ionised and neutral gas residual velocity fields suggest that NW1 is (red) post-shock ionised gas, NW2 is (bluer) shocked ionised gas streaming towards the nucleus similar to the HI shock; SE2 is (blue) pre-shock gas entering the shock and SE1 is (red) shocked gas similar to that seen in HI.

Although the majority of the bright UV emission and associated ionised gas is consistent with pre- and post-shock gas, the NW2 region may represent the unusual case of ionised gas in a bar shock. NW2 coincides with the re-

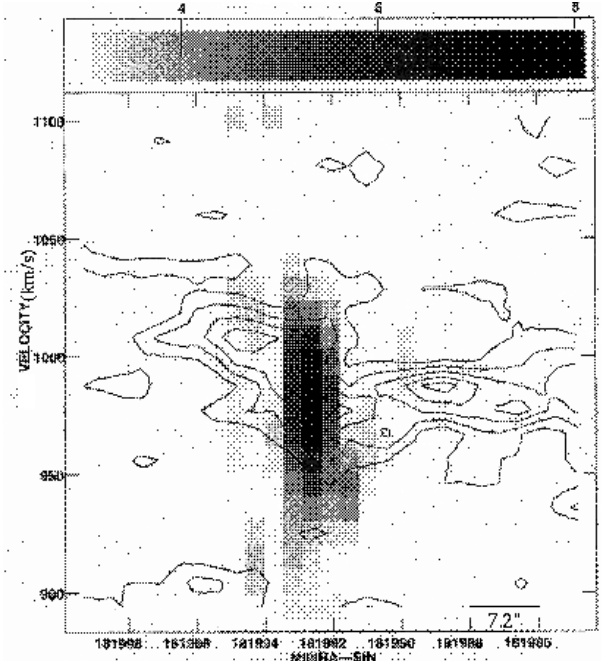


Figure 8. $\text{H}\beta$ (grey-scale) and HI (contour) position-velocity diagrams extracted using a $6''$ -wide slit centred on the $\text{H}\beta$ peak in NW2 and perpendicular to the direction of the shock ridge (see Mundell & Shone 1999).

gion of highest N_H and strongest HI streaming (Mundell & Shone 1999). The much larger concentration of HI in the bar compared to ionised gas allows greater opportunity to look for the sudden jumps in velocity characteristic of gaseous shocks. Nevertheless, we used the same method as Mundell & Shone (1999) to extract the $\text{H}\beta$ emission in a $6''$ -wide slit centred on the $\text{H}\beta$ peak in NW2 and perpendicular to the direction of the shock ridge in order to search for the predicted maximum velocity jump in the ionised gas. Figure 8 shows the resultant position-velocity diagrams of $\text{H}\beta$ (gray-scale) and HI (contour) superimposed; this figure shows that the steep velocity gradient identified in HI data of Mundell & Shone (1999) is also visible in the $\text{H}\beta$ data, further confirming that NW2 represents ionised gas in the shock itself.

We therefore conclude that the distribution of bright UV emission is broadly consistent with the formation of star clusters upstream travelling ballistically through the gaseous shock to ionise gas downstream along the leading edge of bar. In addition, we suggest that ionised gas within the shock itself is detected for the first time and is streaming to smaller radius orbits in the same manner as the neutral gas. Indeed, Reynaud & Downes (1998) find that massive stars cannot form in bar shocks in which the velocity shear is high, as is the case in the HI shocks in NGC 4151 (Mundell & Shone 1999); this further supports our interpretation that although we detect ionised gas in the shock regions, it cannot be ionised by stars formed *in situ* but instead is ionised by stars formed upstream as they pass ballistically through the shock region. The observed kinematics of the brightest HII regions as measured by Schulz (1985), which are consistent with elliptical stellar orbits, are then easily explained.

5 CONCLUSIONS

The TAURUS Fabry-Perot interferometer was used to simultaneously map the distribution and kinematics of H β emission in the Seyfert 1 galaxy NGC4151. The results were compared with that previously determined in neutral hydrogen by Mundell & Shone (1999). We detect for the first time, ionised gas within the shock itself which is streaming to smaller radii in the same manner as the neutral gas.

We suggest that the distribution of bright, patchy UV emission close to the HI shocks is, on the whole, consistent with ionisation by star clusters that have formed in compressed pre-shock gas as they pass ballistically through the shock region. The kinematics are consistent with elliptical stellar orbits. The H β ENLR velocity profile is consistent with previous studies.

6 ACKNOWLEDGEMENTS

The authors are grateful to Steve Unger for the TAURUS observations and for his support of this project in its early stage. We thank Dave Shone and Johan Knapen for useful discussions and Jim Lewis for advice on TAURUS data reduction. CGM acknowledges financial support from the Royal Society. We thank the anonymous referee for constructive comments that helped to improve the paper. The INT is operated on the island of La Palma by the Isaac Newton Group in the Spanish Observatorio del Roque de los Muchachos of the Instituto de Astrofísica de Canarias.

REFERENCES

- Arp H., 1977, *Astrophys. J.*, 218, 70
 Asif M. W., Unger S. W., Pedlar A., Mundell C. G., Robinson A., Walton N. A., 1997, *Mon. Not. R. Astr. Soc.*, 284, L15
 Asif M. W., Mundell C. G., Pedlar A., Unger S. W., Robinson A., Vila-Vilaró B., Lewis J. R., 1998, *Astron. Astrophys.*, 333, 466
 Athanassoula E., 1992a, *Mon. Not. R. Astr. Soc.*, 259, 328
 Athanassoula E., 1992b, *Mon. Not. R. Astr. Soc.*, 259, 345
 Atherton P. D., Taylor K., Pike C. D., Harmer C. F. W., Parker N. M., Hook R. N., 1982, *Mon. Not. R. Astr. Soc.*, 201, 661
 Bland J., Taylor K., Atherton P. D., 1987, *Mon. Not. R. Astr. Soc.*, 228, 595
 Bland-Hawthorn J., Sokolowski J., Cecil G., 1991, *Astrophys. J.*, 375, 78
 Bokernberg A., 1982, *Phil. Trans. R. Soc. Lon. A.*, 307, 531
 Bosma A., Ekers R. D., Lequeux J., 1977, *Astron. Astrophys.*, 57, 97
 Cecil G., Bland J., Tully R. B., 1990, *Astrophys. J.*, 355, 70
 Crenshaw D. M., et al., 2000, *Astrophys. J.*, 120, 1731
 Davies R. D., 1973, *Mon. Not. R. Astr. Soc.*, 161, 25
 de Vaucouleurs G., de Vaucouleurs A., Corwin H. G., Jr. Buta R. J., Paturel G., Fouque P., 1991, Volume 1-3, XII, 2069 pp. 7 figs.. Springer-Verlag Berlin Heidelberg New York
 Elmegreen B. G., 1994, *Astrophys. J. Letters*, 425, 73
 Fanelli M. N., Collins N., Bohlin R. C., Neff S. G., O'Connell R. W., Roberts M. S., 1997, *Astron. J.* 114, 575
 Handa T., Nakai N., Sofue Y., Hayashi M., Fujimoto M., 1990, *PASJ*, 42, 1
 Hutchings J. B. et al., 1999, *Astron. J.*, 118, 2101
 Kuchinski L. E., et al., 2000, *Astrophys. J.S.*, 131, 441
 Lewis J. R., Unger S. W., 1991, in TAURUS Data and How to Reduce It, Royal Greenwich Observatory, Cambridge
 Lindblad P. O., Joersäter S., 1988, in Evolution of Galaxies, ed. J. Palous, (Czech. Acad. Sciences), p. 289
 Lindblad P. A. B., Lindblad P. O., Athanassoula E., 1996, *Astron. Astrophys.*, 313, 65
 Martin P., Friedli D., 1997, *Astron. Astrophys.*, 326, 449
 Martinet L., Friedli D., *Astron. Astrophys.*, 323, 363
 Mason K. O., et al., 2001, *Astron. Astrophys.*, 365, 36
 Menendez-Delmestre K., Sheth K., Scoville N., Jarett T., Schinnerer E., Regan M., Block D. 2004, astro-ph/0407323
 Mundell C. G., Shone D. L., 1999, *Mon. Not. R. Astr. Soc.*, 304, 475
 Mundell C. G., Pedlar A., Shone D. L., Robinson A., 1999, *Mon. Not. R. Astr. Soc.*, 304, 481
 Norman C. A., Sellwood J. A., Hasan H., 1996, *Astrophys. J.*, 462, 114
 Ondrechen M. P., 1985, *Astron. J.*, 90, 1474
 Osterbrock D. E., Koski A. T., 1976, *Mon. Not. R. Astr. Soc.*, 176, 610
 Pedlar A., Howley P., Axon D. J., Unger S. W., 1992, *Mon. Not. R. Astr. Soc.*, 259, 369
 Pedlar A., Kukula M. J., Longley D. P. T., Muxlow T. W. B., Axon D. J., Baum S., O'Dea C., Unger S. W., 1993, *Mon. Not. R. Astr. Soc.*, 263, 471
 Pérez E., González-Delgado R. M., Tadhunter C. N., Tsvetanov Z., 1989, *Mon. Not. R. Astr. Soc.*, 241, 31
 Pérez-Fournon I., Wilson A. S., 1990, *Astrophys. J.*, 356, 456
 Prendergast K. H., 1983, in Internal Kinematics and Dynamics of Galaxies, Proc. IAU Symp. 100, ed. Athanassoula, E., Reidel, Dordrecht, p. 215
 Regan M. W., Vogel S. N., 1995, *Astrophys. J.*, 452, 21
 Regan M. W., Mulchaey J. S., 1999, *Astron. J.*, 117, 2676
 Reynaud D., Downes D., 1998, *Astron. Astrophys.*, 337, 671
 Roberts W. W. Jr. Huntley J. M., Van Albada G. D., 1979, *Astrophys. J.*, 233, 67
 Robinson A., et al., 1994, *Astron. Astrophys.*, 291, 351
 Sakamoto S., Hasegawa T., Handa T., Hayashi M., Oka T., 1997, *Astrophys. J.*, 486, 276
 Schulz H., 1985, *Astron. Astrophys.*, 143, 29
 Schwarz M. P., 1985, *Mon. Not. R. Astr. Soc.*, 212, 677
 Sheth K., Vogel S. N., Regan M. W., Teuben P. J., Harris A. I., Thornley M. D., 2002, *Astron. J.*, 124, 581
 Shlosman I., Frank J., Begelman M. C., 1989, *Nature*, 338, 45
 Spitzer L., Jr. 1978, in Physical Processes in the Interstellar Medium (New York: Wiley)
 Staveley-Smith L., Davies R. D., 1987, *Mon. Not. R. Astr. Soc.*, 224, 953
 Taylor K., Atherton P. D., 1980, *Mon. Not. R. Astr. Soc.*, 191, 675
 Unger S. W., Pedlar A., Axon D. J., Whittle M., Meurs E. J. A., Ward M. J., 1987, *Mon. Not. R. Astr. Soc.*, 228, 671
 Unger S. W., Taylor K., Pedlar A., Ghataure H. S., Penston M. V., Robinson A., 1990, *Mon. Not. R. Astr. Soc.*, 242, 33
 Unger S. W., Lewis J. R., Pedlar A., Axon D. J., 1992, *Mon. Not. R. Astr. Soc.*, 258, 371
 Van Der Kruit P. C., Shostak G. S., 1984, *Astrophys. J.*, 278, 81
 Vila-Vilaró B., et al., 1995, *Astron. Astrophys.*, 302, 58
 Winge C., Axon D. J., Macchett F. D., Capetti A., Marconi A., 1999, *Astrophys. J.*, 519, 134